

An Enhanced Dipole Model Based Micro-Macro Description for Constitutive Behavior of MRFs

Chunwei Zhao^{1,2}, Xianghe Peng^{1,2,3}, Jin Huang⁴ and Ning Hu^{1,5,6}

Abstract: The validity of the two conventional micro-macro descriptions for MRFs, based respectively on the exact dipole model and the simplified dipole model, is examined with the results obtained with the commercially available finite element (FE) code ANSYS. It is found that although the simplified dipole model can match better the result by FE computation, there is still a marked difference. An enhanced dipole model is then suggested, which takes into account the contribution of the magnetized particles to magnetic field. Making use of a statistical approach and neglecting the interaction between particle chains, a micro-macro approach is developed for the evaluation of the yield shear stress of MRFs. It can take into account the effects of all the main influencing factors, and can well replicate the main characteristics of the constitutive behavior of MRFs. The method and the results presented are significant for the analysis and optimization of the mechanical properties of MRFs, and for the design of high-performance MRFs.

Keywords: Magnetorheological fluids; finite element simulation; enhanced dipole model; micro-macro constitutive description

1 Introduction

Magnetorheological fluids (MRFs) are a kind of functional fluids consisting of ferromagnetic particles with micron size suspended in a nonmagnetic carrier fluid. It exhibits as a Newtonian fluid without applying a magnetic field. It could be changed rapidly to a solid-like material once a proper magnetic field is applied, and

¹ Department of Engineering Mechanics, Chongqing University, Chongqing, China

² State Key Laboratory of Coal Mine Disaster Dynamics and Control, Chongqing University, Chongqing, China

³ Corresponding author: Xianghe Peng, *Email address:* xhpeng@cqu.edu.cn

⁴ Chongqing Institute of Automobile, Chongqing University of Technology, Chongqing, China

⁵ Department of Mechanical Engineering, Chiba University, Chiba, Japan

⁶ Corresponding author: Ning Hu, *E-mail address:* huning@faculty.chiba-u.jp

it could be recovered with the removal of the magnetic field. The mechanical property of an MRF could be tuned in a large range with the change of the intensity of the applied magnetic field. Because of these amazing characteristics, MRFs have been receiving increasing attention in the past decades, and have been extensively applied for different purposes, such as vibration control, shock absorbers, buffing attachment, braking devices, etc [Yang *et al.* (2011); Caterino *et al.* (2011); Lee *et al.* (2004); Karakoc *et al.* (2008)].

Great efforts have been made in modeling the constitutive behavior of MRFs. Tang (2000) evaluated the static yield stress with two and three dimensional laminar structure model with the Maxwell stress tensor, which is related to anisotropic magnetization, but it is difficult to be applied in the analysis for practical problems. Rosensweig (1995) developed a mean-field continuum model to analyze the static yield stress without considering demagnetization. Jolly *et al.* (1996) obtained an expression of yield shear stress with the principle of energy conservation. Ginder and Davis (1994) calculated the interaction force in a single chain with a nonlinear finite element method. Later, Ginder (1998) presented a simple model and obtained a set of explicit expressions of the yield stress at different magnetic fields. Bossis and Lemaire (1991) proposed a dipolar sphere model to predict the static yield shear stress of MRFs, however, it may overestimate the yield shear stress due to neglecting the nonlinear magnetization. Based on static magnetics, Si *et al.* (2007) proposed a micromechanics model for the constitutive behavior of MRFs, which takes into account the effects of intensity of applied magnetic field, particle size and particle volume fraction. Peng and Li (2007) formulated a micro–macro constitutive model to predict the static yield stress based on the conventional dipole model and a statistical approach, which can take into account the effects of each of the main influencing factors. Yi *et al.* (2010) investigated the same problem with an exact dipole model without making use of the approximation that the size of the dipolar particles is far smaller than the distance between particles. Although both the two models [Peng and Li (2007); Yi *et al.* (2010)] can take into account the main effect of each individual influencing factor on the overall behavior of MRFs, the yield shear stresses evaluated with the two models exhibit distinct difference. It raises a question: how to evaluate the error when applying a magnetic dipole model in the analysis of MRFs, where the size of the dipolar particles may not be far smaller than the distance between particles. On the other hand, in the conventional magnetic dipole model based analysis, a dipolar particle is usually assumed to be magnetized by the applied magnetic field, and the additional magnetization of the dipole induced by the surrounding magnetic dipoles is often neglected, which may also bring about considerable error as the distance between particles is comparable with the size of the particles.

In order to solve the above problems, in this article, we simulate the magnetization state and the magnetic force of the particles in a single chain under a static magnetic field with the finite element (FE) code ANSYS, where the additional magnetization resulting from the surrounding magnetic dipoles is taken into account. The results are then used as the benchmark to evaluate the results obtained with the conventional magnetic dipole models. An enhanced dipole model is suggested with the consideration of the additional contribution of the magnetized particles to the magnetic field. By virtue of this model, the resistance of a single chain consisting of magnetized particles against shear deformation is obtained. Then a micro-macro description for the yield shear stress of MRFs is formulated by making use of a statistical approach. The typical characteristics of MRFs and the effects of the main influencing factors on the overall constitutive behavior are analyzed. The comparison between the analytical and experimental results demonstrates the validity of the proposed model.

2 Verification of conventional dipole models with FE simulation

2.1 Brief introduction to conventional dipole models

In an MRF, the ferromagnetic particles which are initially distributed randomly in the carrier liquid will be magnetized and become magnetic dipoles if a magnetic field is applied. These dipolar particles may be aligned in the direction of the external magnetic field to form a chainlike microstructure because of the interaction between particles. The evolution of the microstructure under applied magnetic and mechanical fields endows MRFs with unique properties.

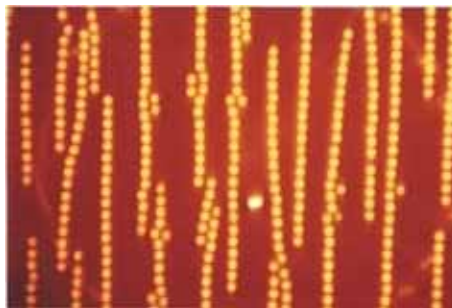


Figure 1: Chainlike microstructure of MRF under magnetic field [Popplewell *et al.* (1996)]

Popplewell *et al.* (1996) and Jolly *et al.* (1996) observed the microstructure morphology of MRFs under an external magnetic field (Figure 1), it can be seen that

the particles are aligned in the direction of the external magnetic field. The chain-like microstructure can hinder the free flow of an MRF and even make an MRF become a material with yield shear stress. Starting from such kind of chainlike microstructure and its deformation pattern during shear deformation (Figure 2), which is similar to the happening mechanism of shear banding in granular materials [Hu and Molinari (2004)], assuming the particles are spheres with identical diameter, and making use of a simplified magnetic dipole model, Peng (2007) obtained the resistance of a single chain against shear deformation as follows

$$T_{sd} = \frac{4A\mu_0}{3k^4} \frac{\pi R^6 \chi^2 H^2}{(2R+2t+\delta)^4} (5 \cos^2 \theta - 1) \cos^4 \theta \sin \theta, \quad (1)$$

where R is the radius of a particle, t is the thickness of the non-magnetic coating, δ is the spacing between the neighboring particles and θ is the angle between the inclined chain and the applied magnetic field, H is the intensity of applied magnetic field, $\mu_0 = 4\pi \times 10^{-7}$ H/m is the permeability in free space, χ is the susceptibility, and A is related to the number of the particles in a single chain, n , with $A|_{n=2} = 1$ and $A|_{n=15} = 1.082 \approx A|_{n \rightarrow \infty}$. In the simplified dipole model, it is assumed that the particle size is far smaller than the distance between particles. Considering that this assumption may not be true in the chainlike microstructure in MRFs, Yi *et al.* (2010) suggested an exact dipole model without making use of the assumption, with which the corresponding resistance was obtained as

$$T_{ed} = \sum_{k=1}^{n-1} \frac{2}{3} E_k \mu_0 \pi R^5 \chi^2 H^2 \cos^4 \theta \sin \theta \quad (2)$$

where

$$E_k = \sum_{i=0}^1 \frac{k(2R+2t+\delta) [k(2R+2t+\delta) + (-1)^i R]}{\left\{ [k(2R+2t+\delta)]^2 + R^2 \cos^2 \theta + (-1)^i 2kR(2R+2t+\delta) \cos^2 \theta \right\}^{\frac{5}{2}}}. \quad (3)$$

2.2 FE Simulation

In the module of Multiphysics in FE code ANSYS, the Maxwell equations are adopted for electromagnetic field analysis. The characteristics of the particles in an MRF can be simulated and the magnetic force on a particle can be obtained by integrating the Maxwell stress tensor over the surface elements of the particle. It should be a more accurate method, especially for the case of nonlinear magnetizing process, because it can take into account the effect of the distribution of magnetization and realistic interaction between magnetized particles, and can tackle more complex initial and boundary conditions.

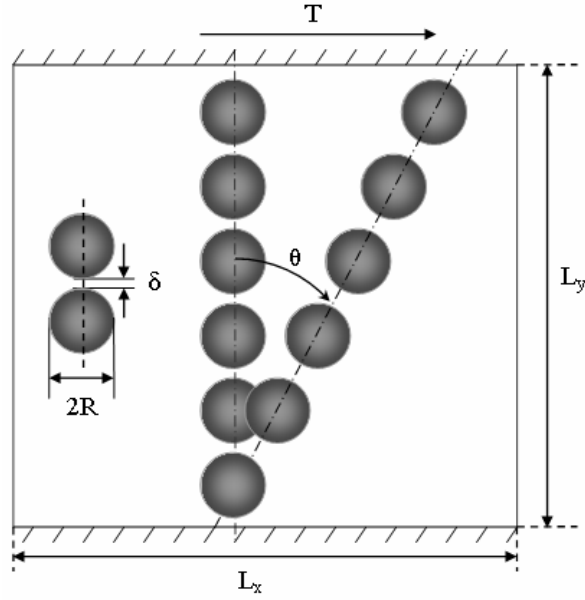


Figure 2: Shear deformation of a single chain

An electromagnetic field is governed by the following Maxwell equations

$$\nabla \times \mathbf{H} = \mathbf{J} + \frac{\partial \mathbf{D}}{\partial t}, \quad (4)$$

$$\nabla \times \mathbf{E} = -\frac{\partial \mathbf{B}}{\partial t}, \quad (5)$$

$$\nabla \cdot \mathbf{B} = 0, \quad (6)$$

$$\nabla \cdot \mathbf{D} = \rho, \quad (7)$$

where \mathbf{H} denotes magnetic field intensity, \mathbf{J} current density, \mathbf{E} electric field intensity, \mathbf{B} magnetic flux density, \mathbf{D} electric flux density, and ρ is magnetic charge density. For an applied static magnetic field, $\mathbf{J}=\mathbf{0}$ and $\mathbf{D}=\mathbf{0}$, the Maxwell equations can be rewritten as

$$\nabla \times \mathbf{H} = 0, \quad (8)$$

$$\nabla \cdot \mathbf{B} = 0. \quad (9)$$

The constitutive relation for the electromagnetic materials is

$$\mathbf{B} = \mu_0 (\mathbf{H} + \mathbf{M}) = \mu_0 (1 + \chi) \mathbf{H} \quad (10)$$

where $\mathbf{M} = \chi\mathbf{H}$ is the intensity of magnetization, χ is the susceptibility, μ_0 is the permeability in free space. The Maxwell stress tensor can be expressed as [Yan (2006)]

$$S_{ij} \equiv \epsilon_0 \left(E_i E_j - \frac{1}{2} \delta_{ij} E^2 \right) + \frac{1}{\mu_0} \left(B_i B_j - \frac{1}{2} \delta_{ij} B^2 \right) \tag{11}$$

where δ_{ij} is the Kronecker symbol.

For 3-D application, the Maxwell forces can be obtained in the following surface integral

$$\{\mathbf{F}^{mx}\} = \frac{1}{\mu_0} \oint_s [\mathbf{S}] \{\mathbf{n}\} ds = \frac{1}{\mu_0} \oint_s \begin{bmatrix} B_x^2 - \frac{1}{2}|B|^2 & B_x B_y & B_x B_z \\ B_x B_y & B_y^2 - \frac{1}{2}|B|^2 & B_y B_z \\ B_x B_z & B_y B_z & B_z^2 - \frac{1}{2}|B|^2 \end{bmatrix} \{\mathbf{n}\} ds \tag{12}$$

where s is the surfaces of the ferromagnetic regions and \mathbf{n} is the unit outward normal vector of the surface.

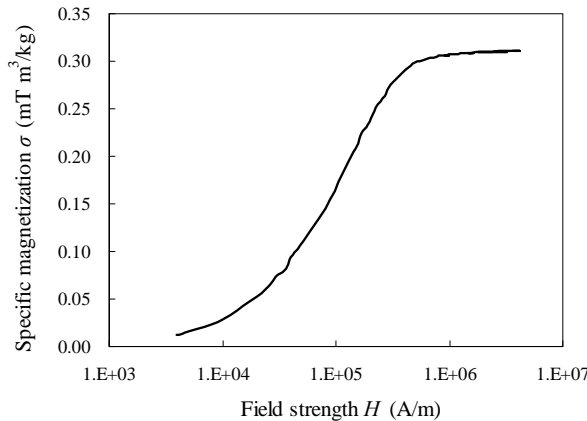


Figure 3: Variation of specific magnetization against magnetic field intensity of particle material [Bombard (2005)]

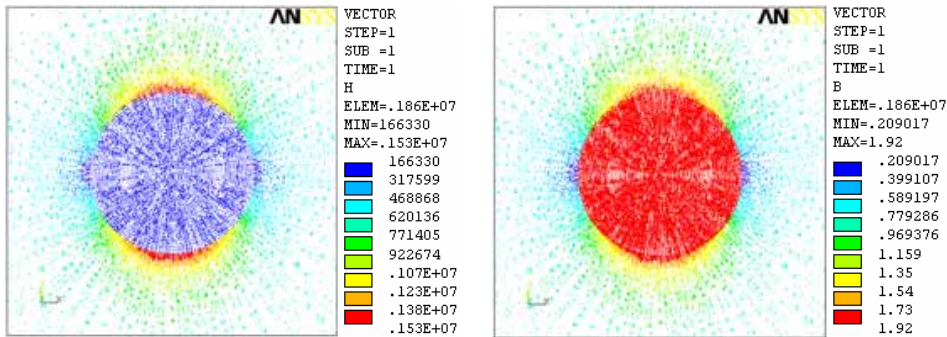
2.3 Comparison

In order to calculate the forces of a single chain in MRFs, we established a particles-air system. A particle chain is located at the center of the air, and a uniform upward magnetic field is applied in the air. In the following, a 3D magnetic scalar potential and the magnetic scalar potential method are used to analyze the magnetic field.

The parameters used are listed in Table 1, where δ is the gap between particles, which can be regarded as the thickness of the oil-film, and t is the thickness of non-ferromagnetic coating. The variation of specific magnetization against magnetic field intensity of the particle material [Bombard (2005)] is shown in Figure 3. The density of the particle material is about $7.8 \times 10^3 \text{ kg/m}^3$, the intensity of the magnetic field $H \approx 633 \text{ kA/m}$, and the susceptibility $\chi = 1.96$.

Table 1: Model parameters (μm)

x	y	z	R	δ	t
300	300	60	6	1.2	0.4



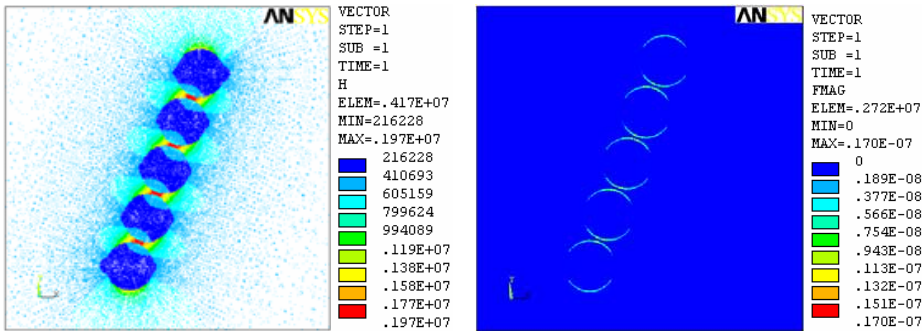
(a) Vectorgraph of magnetic field intensity (A/m) (b) Vectorgraph of magnetic induction (T)

Figure 4: Vectorgraphs of magnetic field intensity and magnetic induction in/near a single particle

The magnetization of a particle or a particle chain is simulated with the FE code ANSYS. The computed vectorgraphs of the intensities of the magnetic field and the magnetic induction of a single particle are shown in Figures 4(a) and 4(b), respectively. It can be seen that, the intensity of the magnetic field is almost uniform inside the particle, but far smaller than the intensity of the applied magnetic field. However, although the intensity of the magnetic induction is also almost uniform inside the particle, it is larger than that in the surrounding air. The maximum intensity of the magnetic field outside of the particle is much larger than that of the applied magnetic field, which would be attributed to the disturbance of the magnetized particle, i.e., the induced magnetic field inside the magnetized particle is

opposite to the applied magnetic field. Since the magnetic susceptibility of the particle is larger than that of the air, the magnetic induction inside the particle is larger than that outside the particle. The intensity of the magnetic field surrounding the particle decreases rapidly with the increase of the distance and tends to that of the applied magnetic field.

Figures 5(a) and 5(b) show the computed distributions of the magnetic field intensity and the induced Maxwell stress when a single chain of five particles is placed in the applied static magnetic field, which is inclined with 20° from the direction of applied magnetic field. It can be seen that, because of the interaction of magnetized particles, the intensity of the magnetic field in each of the particles increases significantly compared with that of a single particle, with the maximum value appearing at the minimum spacing between two particles. The Maxwell stress is related to the magnetic field intensity, which is the superposition of the applied magnetic field intensity and the additional magnetic field caused by the magnetized particles. The maximum value of the Maxwell stress appears at the maximum value of the magnetic field intensity. If the particles from top to bottom are numbered sequentially with P1 to P5, the interaction force between neighboring particles is shown in Figure 6, in which it can be seen that P2-3 and P3-4 are a little larger, due to the involvement of the magnetic interaction between particles 1 and 3, and between 5 and 3, respectively.



(a) Vectorgraph of magnetic field intensity (A/m) (b) Vectorgraph of Maxwell stress (N/m²)

Figure 5: Vectorgraphs of magnetic field intensity and Maxwell stress in a single chain

During a shearing process, a chain is stretched and inclined, and the contribution of the chain to the resistance against the shearing deformation is the horizontal

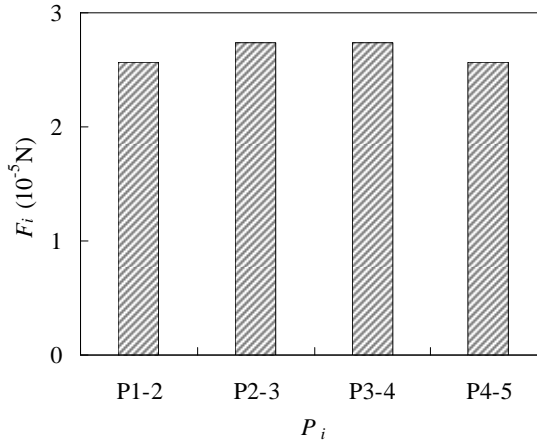


Figure 6: Interaction force between neighboring particles

component of the magnetic force, T . Making use of the deformed single chain shown in Figure 2, given a set of θ , the corresponding T can be computed. The relation between T and θ is computed and shown in Figure 7, the corresponding results obtained with two kinds of dipole models are also shown for comparison. Taking the FE result as a benchmark, it can be seen that the exact dipole model (EDM) over-predicts the response, while the simplified dipole model (SDM) a little under-predicts the response. This is because that in the dipole model a magnetized particle is simplified as a magnetic dipole, which is an approximation that may enhance the effect of the magnetization. In SDM the assumption that the particle size is much smaller than the distance between particles may partly counteract the enhancement, while in EDM no such assumption is employed so that the over-prediction due to the enhancement of the dipole model could not be erased.

In order to describe the continuously metabolic process in MRFs under a static magnetic field, we assume sufficient particle chains per unit area and the normal distribution of θ (Figure 2), and obtain the macroscopic yield shear stress of an MRF contributed by these chains, $\bar{\tau}$, as the summation of the contributions of these chains [Peng and Li (2007)]. The variations of $\bar{\tau}$ against γ can be obtained and shown in Figure 8, where it can be seen that $\bar{\tau}$ increases with the increase of γ until reaching to the maximum value. It can be seen that, compared with the result obtained with EDM, the results obtained with SDM better match the results obtained by the finite element method (FEM). However, remarkable difference between the saturated yield shear stress by SDM and that by FEM can also be found, indicating the necessity of the modification of the dipole model.

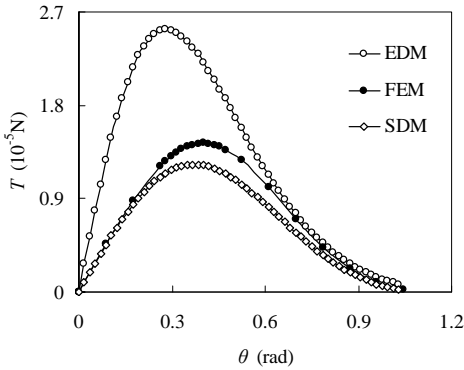


Figure 7: Variation of T against θ of a single chain

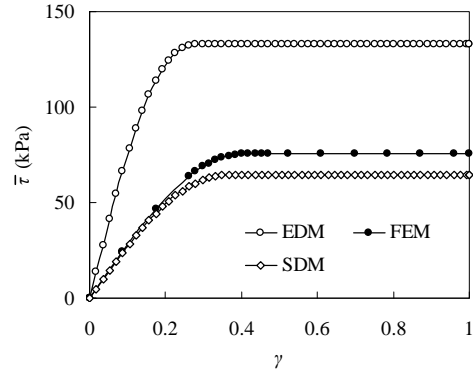


Figure 8: Variation of $\bar{\tau}$ against γ of an MRF

3 Enhanced dipole model

According to the study by Furst (2000), under an external magnetic field, the particles will be magnetized and an additional magnetic field will be induced around and superimposed on the applied magnetic field at the location of each particle. Therefore, it should be noted that, the magnetic field at the location of a particle should be the summation of the additional magnetic field induced by all the neighboring dipoles and the applied magnetic field. In the conventional dipole models [Peng and Li (2007); Yi *et al.* (2010)], the additional magnetization of a dipole induced by the other magnetic dipoles is often neglected, which may lead to an incorrect evaluation. Thus, an enhanced dipole model will be developed by taking into account the effect of this additional magnetic field.

The magnetic moment of a conventional dipole of radius R can be expressed as [Wan *et al.* (1994)]

$$\mathbf{m} = V\mathbf{M} = \frac{4}{3}\pi\chi R^3\mathbf{H} \quad (13)$$

where $V = 4/3\pi R^3$ is the volume of the particle, \mathbf{H} is the magnetic field, $\mathbf{M} = \chi\mathbf{H}$ is the intensity of the magnetization and χ is the susceptibility.

The magnetic field intensity of a dipolar particle can be expressed as [Li (2006)]

$$\mathbf{H} = \frac{1}{4\pi} \left[\frac{3(\mathbf{m} \cdot \mathbf{r})\mathbf{r}}{r^5} - \frac{\mathbf{m}}{r^3} \right] \quad (14)$$

Substituting equation (13) into (14), the additional magnetic field intensity at Point

i induced by Dipolar particle j can be expressed as

$$\mathbf{H}_j^{(i)} = \chi R^3 \left[\frac{(\mathbf{H} \cdot \mathbf{r}_{ij}) \mathbf{r}_{ij}}{r_{ij}^5} - \frac{\mathbf{H}}{3r_{ij}^3} \right] \quad (15)$$

where R is the radius of particle, and \mathbf{r}_{ij} is the vector from Particle i to Particle j .

The total magnetic field at Particle i can be expressed as

$$\mathbf{H}_i = \mathbf{H}_0 + \sum_{j \neq i}^{(i)} \mathbf{H}_j = \mathbf{H}_0 + \chi R^3 \sum_{j \neq i} \left[\frac{(\mathbf{H}_0 \cdot \mathbf{r}_{ij}) \mathbf{r}_{ij}}{r_{ij}^5} - \frac{\mathbf{H}_0}{3r_{ij}^3} \right] \quad (16)$$

where $\mathbf{H}_0 = H\mathbf{k}$ is the applied uniform magnetic field intensity, and \mathbf{k} denotes the direction of the applied magnetic field.

The intensity of the magnetic induction at Particle i , i.e., \mathbf{B}_i , can be expressed as

$$\mathbf{B}_i = \mu_0 \mathbf{H}_i \quad (17)$$

where $\mu_0 = 4\pi \times 10^{-7} \text{Hm}^{-1}$ is the permeability in free space.

Assuming all particles are of spheres of the same size, the potential of a magnetic dipoles-system can be expressed as

$$U = -\frac{1}{2} \sum_i \mathbf{m}_i \cdot \mathbf{B}_i = -\frac{2}{3} \pi \mu_0 \chi R^3 \sum_i \mathbf{H}_i \cdot \mathbf{H}_i \quad (18)$$

Then the magnetic force on Particle j can be derived as

$$\mathbf{F}_j = -\nabla U = \sum_{i \neq j}^{(j)} \frac{4\mu_0 \pi H^2 \chi^2 R^6}{3r_{ij}^5} \left\{ \left[(1 - 5 \cos^2 \theta_i) - \frac{\chi R^3}{3r_{ij}^3} (1 + 4 \cos^2 \theta_i) \right] \mathbf{r}_{ij} + 2r_{ij} \cos \theta_i \left[1 + \frac{\chi R^3}{6r_{ij}^3} \right] \mathbf{k} \right\} \quad (19)$$

Making use of Eq. (19) the contribution of the chain inclined with θ_i from \mathbf{H}_0 (Figure 2) to the resistance against shear deformation of an MRF can be obtained as

$$T_i = \sum_{j=1}^{n-1} \frac{4\mu_0 \pi H^2 \chi^2 R^6}{3r_j^4} \left[(1 - 5 \cos^2 \theta_i) - \frac{\chi R^3}{3r_j^3} (1 + 4 \cos^2 \theta_i) \right] \sin \theta_i \quad (20)$$

where n is the number of the particles in the chain.

The macroscopic yield shear stress of an MRF can be obtained as

$$\tau = \tau_0 + \bar{\tau} \quad (21)$$

where τ_0 is the shear stress without applying a magnetic field. If the normal distribution of θ_i is assumed [Peng and Li (2007)] and the interaction between chains is neglected, one has

$$\bar{\tau} = \sum_{j=1}^{n-1} \frac{\mu_0 \phi H^2 \chi^2 R^3 (2R + \delta)}{r_j^4} \int_{-\frac{\pi}{2}}^{\frac{\pi}{2}} \left[(1 - 5 \cos^2 \theta) - \frac{\chi R^3}{3r_j^3} (1 + 4 \cos^2 \theta) \right] \sin \theta \times \frac{1}{\sqrt{2\pi\sigma}} e^{-\frac{(\theta-\mu)^2}{2\sigma^2}} d\theta \quad (22)$$

where ϕ is the particle volume fraction, δ is the gap between particles, μ and σ are the mean and the standard error, respectively, which could be related to shear strain and its rate [Peng and Li (2007)].

It can be seen that the effects of the magnetic field intensity, the radius of particle, the distance between particles, strain and strain rate on the yield shear stress can be considered in this model, which should be significant for the evaluation of the yield shear stress and the design of high-performance MRFs.

4 Simulation and verification

The variations of T_{max} against n of a single chain are shown in Figure 9, where T_{max} is the maximum of T and n is the number of the particles in a single chain. It can be seen that T_{max} increases with the increase of n and almost reaches a saturated value at $n=5$. It indicates that $n=5$ can meet the requirement of accuracy for the single-chain structure. It can be seen that result obtained by the enhanced dipole model (ENDM) is in good coincidence with that obtained by FEM, and is much better than that given by SDM.

Base on the deformed configuration of a single chain (Figure 2), the variations of T against θ can be obtained and shown in Figure 10. Compared with the results obtained with SDM, the results obtained by ENDM can match those obtained by FEM better.

The variation of $\bar{\tau}$ against γ of an MRF ($\phi = 0.36$) calculated with Eq. (23) is shown in Figure 11, and the results corresponding to SDM and FEM are also given for comparison. It can be seen that, compared with the result given by SDM, the result given by ENDM can better replicate the result obtained by FEM, demonstrating the validity for ENDM's applications in the analysis of the mechanical properties of MRFs.

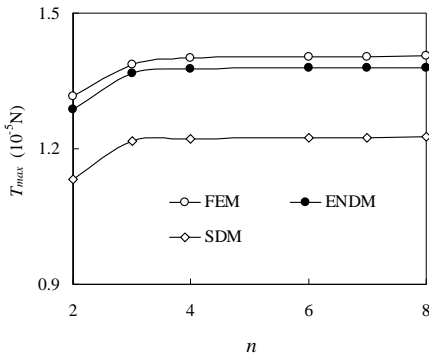


Figure 9: Variation of T_{max} against n of a single chain

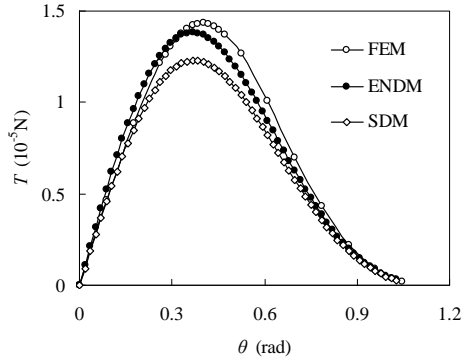


Figure 10: Variation of T against θ of a single chain

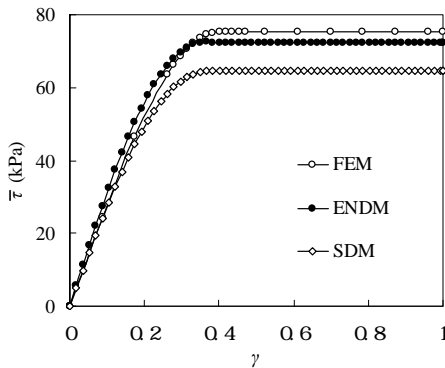


Figure 11: Variation of $\bar{\tau}$ against γ of an MRF

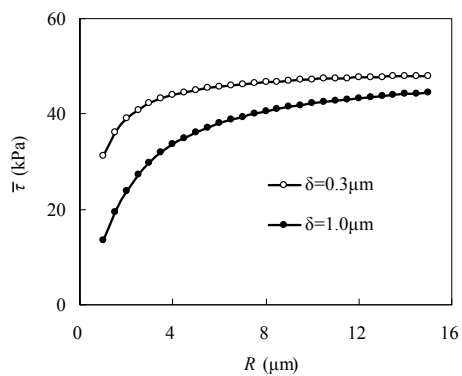


Figure 12: Variation of $\bar{\tau}$ against R of an MRF

4.1 Effect of particle sizes

The variations of $\bar{\tau}$ against R (Figure 12) can be estimated with Eq. (22), where $\phi = 0.4$, $\chi=3.0$, $H=455\text{kA/m}$, $\mu=0.2$, $\sigma=0.1$. It can be seen that $\bar{\tau}$ increases with the increase of R , $\bar{\tau}$ tends to be independent of R as R is sufficiently large, which agrees with the experimental observation by Lemaire *et al.* (1995).

4.2 Effect of particle volume fraction

The variations of $\bar{\tau}$ against ϕ can be expressed as $\tau \approx \bar{\tau} = \vartheta\phi$, where

$$\vartheta = \sum_{j=1}^{n-1} \frac{\mu_0 H^2 \chi^2 R^3 (2R + \delta)}{r_j^4} \int_{-\frac{\pi}{2}}^{\frac{\pi}{2}} \left[(1 - 5 \cos^2 \theta) - \frac{\chi R^3}{3r_j^3} (1 + 4 \cos^2 \theta) \right] \sin \theta \times \frac{1}{\sqrt{2\pi\sigma}} e^{-\frac{(\theta-\mu)^2}{2\sigma^2}} d\theta \quad (23)$$

The variations of $\bar{\tau}$ against ϕ at $B=3kGs$ is shown in Figure 13 where $\vartheta = 17.7kPa$ is identified. It can be seen that in the range of the prescribed particle volume fraction, the linear relationship between $\bar{\tau}$ and ϕ can reasonably describe the dependence of $\bar{\tau}$ on ϕ . The tendency is basically in conformity with the experiment result [Chang (2001)] if ϕ is relatively small. It can also be seen that the results obtained by ENDM can reasonably replicate that obtained in experiment (EXP) [Chang (2001)] as $\phi < 20\%$. According to the experimental study by Rong *et al.* (2000), an MRF exhibits dominantly chainlike microstructure if ϕ is small; however, the microstructure of an MRF may turn to be pilelike if ϕ is large. On the other hand, the interaction between particle chains may not be neglected when ϕ is very large. These can account for the difference between the calculated result and the experimental result.

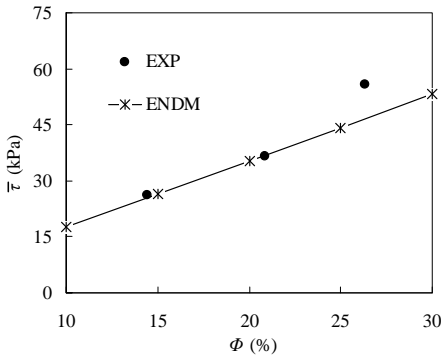


Figure 13: Variation of $\bar{\tau}$ against ϕ of an MRF

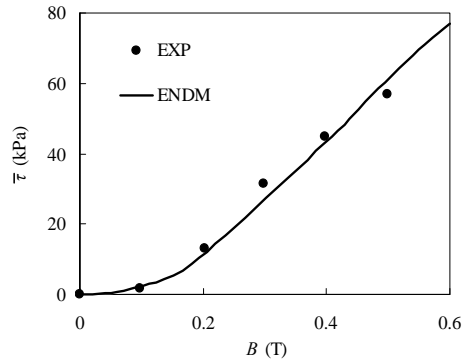


Figure 14: Variation of $\bar{\tau}$ against B of an MRF

4.3 Effect of magnetic induction intensity

The variation of $\bar{\tau}$ against B at $\phi=0.26$, $R=8\mu m$, $\delta=0.2\mu m$, $\mu=0.22$, $\sigma=0.011$ is analyzed and compared with the experiments data [Liu *et al.* (2004)], as shown in

Figure 14. Keeping in mind the equation $\mathbf{B} = \mu_0(1 + \chi)\mathbf{H}$, and the variation of $\bar{\tau}$ against B can be expressed as

$$\tau \approx \bar{\tau} = \sum_{j=1}^{n-1} \frac{\phi B^2 \chi^2 R^3 (2R + \delta)}{\mu_0 (1 + \chi)^2 r_j^4} \int_{-\frac{\pi}{2}}^{\frac{\pi}{2}} \left[(1 - 5 \cos^2 \theta) - \frac{\chi R^3}{3r_j^3} (1 + 4 \cos^2 \theta) \right] \sin \theta \times \frac{1}{\sqrt{2\pi\sigma}} e^{-\frac{(\theta-\mu)^2}{2\sigma^2}} d\theta \quad (24)$$

The relationship $\chi = \chi(H)$ can be identified experimentally [Liu *et al.* (2004)]. It can be seen that $\bar{\tau}$ increases with the increase of B and the yield shear stress obtained by ENDM is in reasonable agreement with the experiments result [Liu *et al.* (2004)].

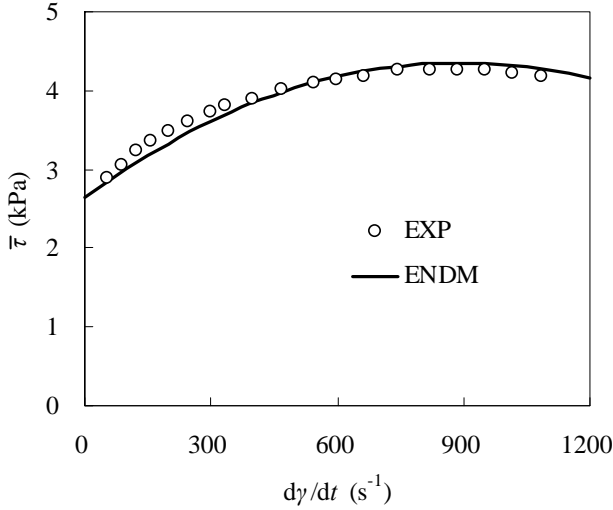


Figure 15: Variation of $\bar{\tau}$ against dy/dt of an MRF

4.4 Effect of shearing rate

Assuming $\mu = c_a + c_2(\dot{\gamma})$ [Peng and Li (2007)], where c_a is a constant and $c_2(\dot{\gamma}) = c_i \dot{\gamma}$. The variations of $\bar{\tau}$ against $\dot{\gamma}$ can be determined. For $\phi = 0.2$, with the material parameters determined with experimental result [Cheng *et al.* (2003)]: $H=109\text{kA/m}$, $\sigma = 1.6$, $c_a = 0.65$ and $c_i = 0.0011\text{s}$, the variation of $\bar{\tau}$ against $\dot{\gamma}$ of the MRF is calculated and shown in Figure 15. The comparison with the experiments result [Cheng *et al.* (2003)] shows satisfactory agreement. It can be seen that at a small $\dot{\gamma}$ the

critical shear stress increases rapidly with the increase of $\dot{\gamma}$, but the slope decreases gradually. It tends to be close to the maximum value at a certain $\dot{\gamma}$, then it falls as $\dot{\gamma}$ is sufficiently large. This tendency agrees with the experiments data [Cheng *et al.* (2003)].

5 Conclusions

The magnetization of and the magnetic force on a ferromagnetic particle and a chain consisting of several ferromagnetic particles in a static magnetic field are computed respectively with the commercially available FE code ANSYS, with which the validity of the application of the two conventional dipole models, i.e., the exact dipole model and the simplified dipole model, in the analysis of the magneto-mechanical property of MRFs is examined. It is found that although the simplified dipole model can match the result by FE computation better, there is still a remarkable difference.

For this reason, an enhanced dipole model is developed for the analysis of the magnetization of and the magnetic force on ferromagnetic particles, which takes into account the effect of the magnetized particles on a magnetic field. Making use of a statistical approach and neglecting the interaction between particle chains, a micro-macro approach is developed for the evaluation of the yield shear stress of MRFs.

The significance of the developed approach lies in the following three aspects: (1) It evaluates the error when a magnetized particle is simplified as a dipole and used in the analysis for the mechanical property of MRFs; (2) It is shown that, among the three dipole model, the enhanced dipole model can match the result obtained by FE computations best; And (3) the developed approach can take into account individually the effects of all the main influencing factors on the mechanical property of MRFs, and can well replicate the main characteristics of the constitutive behavior of MRFs observed in experiments. Therefore, the method and the results presented are significant for the analysis and optimization of the mechanical properties of MRFs, and for the design of high-performance MRFs.

Acknowledgement: The authors gratefully acknowledge the financial support to this work from NSFC under Grant Number 10872220, Chongqing Science and Technology Commission under Grant No. 2011BA4028, and the Fundamental Research Funds for the Central Universities under Grant Number CDJXS11240005.

References

- Bombard A.** (2005): Experimental study of MR suspensions of carbonyl iron powders with different particle sizes. *International Journal of Modern Physics B*, vol. 19, pp. 1332-1338.
- Bossis G.; Lemaire E.** (1991): Yield stresses in magnetic suspensions. *Rheol*, vol. 35, pp. 1345-1347.
- Caterino N.; Spizzuoco M.; Occhiuzzi A.** (2011): Understanding and modeling the physical behavior of magnetorheological dampers for seismic structural control. *Smart Mater. Struct.* vol. 20, pp. 1-19.
- Chang J.; Yang Y.; Peng X.; Huang S.** (2001): Research on a Magnetorheological Fluid Rheological Property Testing Device. *Sci. Instrum*, vol. 22, pp. 354-358.
- Cheng H.; Li L.; Guan J.; Tao J.; Zhang Q.; Yuan R.** (2003): Rheological characteristics of Fe/Fe₃O₄ nanocomposite-based magnetorheological suspension. *China Powder Science and Technology*, vol. 9, pp. 22-25.
- Furst E.; Gast A.** (2000): Micromechanics of magnetorheological suspensions. *Phys. Rev. E*, vol. 61, pp. 6732-6739.
- Ginder J.** (1998): Behavior of magnetorheological fluids. *MRS Bull*, vol. 23, pp. 26-29.
- Ginder J.; Davis L.** (1994): Shear stresses in magnetorheological fluids: role of magnetic saturation. *Appl. Phys. Lett*, vol. 65, pp. 3410-3416.
- Hu N.; Molinari J. F.** (2004): Shear banding in dense metallic granular materials. *Journal of the Mechanics and Physics of Solids*, vol. 52, pp. 499-531.
- Jolly M.; Carlson J.; Muñoz B.** (1996): A model of the behavior of magnetorheological materials. *Smart Materials & Structures*, vol. 5, pp. 607-614.
- Karakoc K.; Park E. J.; Suleman A.** (2008): Design considerations for an automotive magnetorheological brake. *Mechatronics*, vol. 18, pp. 434-447.
- Lee S.; Lee J.; Kim W.; Yook Y.; Kim J.** (2004): Conductor-loss reduction for high-frequency transmission lines based on the magnetorheological-fluid polishing method. *Microwave and Optical Technology Letters*, vol. 42, pp. 405-407.
- Lemaire E.; Meunier A.; Bossis G.; Liu J.; Felt D.; Bashtovoi P.; Matoussevitch N.** (1995): Influence of the particle size on the rheology of magnetorheological fluids. *Rheol*, vol. 39, pp. 1011-1020.
- Li H.** (2006): The characteristics analysis and microscopic mechanism research of magnetorheological fluid. *PhD. Dissertation of Chongqing University*.
- Liu Q.; Tang L.; Zhang P.** (2004): Study on practical magnetorheological fluid. *Journal of Functional Materials*, vol. 35, pp. 291-292.

Peng X.; Li H. (2007): Analysis of the magnetomechanical behavior of MRFs based on micromechanics incorporating a statistical approach. *Smart Materials and structures*, vol. 16, pp. 2477-2485.

Popplewell J.; Rosensweig R. (1996): Magnetorheological fluid composites. *Phys. D: Appl. Phys.*, vol. 299, pp. 2297-2303.

Rong Y.; Tao R.; Tang X. (2000): Experimental Study on Magnetorheological Fluids. *International Journal of Advanced Manufacturing Technology*, vol. 16, pp. 822-829.

Rosensweig R. (1995): On magnetorheology and electrorheology as status of unsymmetric stress. *Rheol*, vol. 39, pp. 179-192.

Si H.; Peng X.; Li X. (2008): A micromechanical model for magnetorheological fluids. *Intell. Mater. Syst. Struct*, vol.19, pp. 19-23.

Tang X.; Conrad H. (2000): An analytical model for magnetorheological fluids. *Phys. D: Appl. Phys.* Vol. 33, pp. 3026–3032.

Wan F.; Ma X. (1994): Magnetic Physics. *Beijing: Electric Industry Press*.

Yan Z. (2006): ANSYS10.0 Engineering electromagnetic analysis technology and example explanation. *Beijing: Press of China Water Conservancy & Hydroelectricity*.

Yang M.; Chen Z.; Hua X. (2011): An experimental study on using MR damper to mitigate longitudinal seismic response of a suspension bridge. *SOIL DYN EARTHQ ENG*, vol. 31, pp. 1171-1181.

Yi C.; Peng X.; Zhao C. (2010): An magnetic-dipoles based micro- macro constitutive model for MRFs subjected to shear deformation. *Rheol Acta*, vol. 49, pp. 815-825.